Controlling the Structure and Rheology of Polyimide/Nanoclay Composites by Condensation Polymerization

Jia Wang, Jude O. Iroh, Amy Long

Materials Engineering Program, School of Aerospace systems, University of Cincinnati, Cincinnati, OH 45221

Received 13 July 2010; accepted 6 June 2011
DOI 10.1002/app.36242
Published online 31 January 2012 in Wiley Online Library (wileyonlinelibrary.com).

ABSTRACT: A novel *in situ* condensation polymerization method for controlling the structure and dispersion of clay in the polyimide (PI) matrix has been investigated. Initially, the viscosity of the polymerizing poly(amic acid) (PAA) solution increases rapidly with increasing shear rate and polymerization time. In the presence of clay, the PAA solution viscosity became significantly higher than that for the neat PAA solution at initial polymerization stage; however, it attained a final value, which was significantly lower than that for a neat PAA solution after a long polymerization time. The PAA/clay solution synthesized by *in situ* polycondensation reaction also showed an interesting optical activity between 500 and 600 nm. The PAA/clay solution prepared by a two-step method involving polymerization followed by the addition of clay shows no unusual optical behavior above 400 nm. The imidization of PAA is enhanced in the presence of clay. The imidization temperature decreased significantly in the presence of clay, and the extent of imidization increased with increasing amount of clay and cure temperature. X-ray diffraction and microscopy studies show the existence of exfoliated clays at low concentration of clay and at high curing temperatures. © 2012 Wiley Periodicals, Inc. J Appl Polym Sci 125: E486–E494, 2012

Key words: polyimide; organoclay; composites; dispersion; optical properties

INTRODUCTION

High-performance polymers like polyimide (PI) have gained interests in both academia and industries due to their outstanding tensile strength and elastic modulus, high-thermal stability, and good resistance to organic solvents.[1] The properties of PI and its precursor poly(amic acid) (PAA) can be significantly enhanced by incorporating reinforcing fillers with high-aspect ratios, such as layered silicate clays. Organoclay, such as montmorillonite (MMT) clay, is the organically modified sodium clay and has improved compatibility, hence higher efficiency of reinforcement, with the polymer matrix.

MMT has a crystal structure consisting of two-dimensional hydrated alumino-silicate layers. Each layer has a thickness of 10 Å and contains an alumina octahedral sheet sandwiched between two silica tetrahedral sheets. Stacking of these layers leads to van der Waals gaps (galleries).[2–6] The exceptionally high-aspect ratio of clay platelets in nanoscale enables enhanced properties to polymer/nanoclay composites when compared with the pristine polymer matrices, including higher modulus,[7–9] increased thermal stability and conductivity,[9–12] improved solvent resistance,[13] and ionic conductivity,[14] and enhanced self-passivation.[15] In addition, it is widely believed that polymer composites containing well-dispersed organoclay nanofillers show significantly improved barrier properties due to an increased tortuosity of the penetration path of an ingressive fluid and improved hydrophobicity of the polymer matrix.[9,16,17] The performance of PI/nanoclay composites vary widely depending on the level of clay dispersion, the size of the alkylated ammonium ions, the reactive functional groups present in the clay, and the polymer matrix.[18–22]

Studies have been conducted with the aim of improving the dispersion of clay in a polymer matrix. Delozier et al.[19] used *in situ* polymerization technique to improve the elastic modulus and the clay dispersion of PI/clay composites. Agglomeration and poor dispersion of clay in the polymer matrix were observed on the addition of clay to a fully formed PAA (*ex situ* polymerization), and *in situ* polymerization was proved to benefit the dispersion of clay.[19,20,23–25]

In situ intercalation condensation polymerization is used in this study to improve the dispersion of layered-silicate clay in a PI matrix. Also present are effects of varying clay content and imidization procedure on the dispersion and structure of clay in a

Correspondence to: J. O. Iroh (irohj@ucmail.uc.edu).

Contract grant sponsor: CMS Division of National Science Foundation (NSF); contract grant number: NSF-CMMI-0758656.

Contract grant sponsor: Research Experience for Undergraduate Supplemental Grant; contract grant number: NSF-CMMI-0934334.

PI matrix. PAA/nanoclay composites cured at a moderate-to-high temperature, $T \geq 150°C$, contains well-dispersed clays, composed of both exfoliated and intercalated clays, which has not been fully reported in the previous literatures. The effect of polymerization time on the rheological behaviors of the polymerizing 4,4′-oxydianiline (ODA)/pyromelittic dianhydride (PMDA) solution with and without clay is determined and correlated with the synthesis conditions. The presence of clay during condensation polymerization was shown to expedite and improve the polymerization of PI. An unusual optical activity was discovered in the PAA/nanoclay suspension prepared by a one-step *in situ* condensation intercalation polymerization due to the presence of radical cations and terminal-conjugated structure in the PI molecules. This phenomenon is similar to that exhibited by a conjugated polymer such as doped polyaniline and imparts possible application of PI/clay coatings and thin films in the areas of corrosion inhibition, chemical sensing, and related technologies.

EXPERIMENTAL

Preparation of PI/nanoclay composite coatings and thin films

Cloisite 15A clay used in this experiment is natural MMT clay modified with dimethyl dehydrogenated tallow quaternary ammonium ion and was purchased from Southern Clay Products. The monomers, ODA (97%), and PMDA (99% pure) and solvent 1-methyl-2-pyrrolidinone (NMP), were purchased from Aldrich Chemical Company. To prepare neat PI solutions, 0.025 mol of ODA was dissolved in 100 mL of NMP and placed in a three-necked flask maintained at 10°C with stirring for 30 min followed by the addition of equimolar amount of PMDA. Polymerization was carried out for a time of 15 h under continuous stirring in a three-necked flask. For the synthesis of PI/nanoclay composite using *in situ* condensation polymerization method, clay was mixed with ODA solution, and the set-up was kept stirred for 6 h, followed by the addition of equimolar PMDA and continuous stirring for 15 h. The polymerization reaction took place at the presence of clay. The concentration of clay in the reaction mixture was varied from 0.2 to 2 wt %. PAA/clay composite solutions were also prepared for comparison following the same route except that the clay was added into the already fully polymerized PAA solutions. Both the neat polymer and composite solutions prepared by *in situ* condensation polymerization were ultrasonicated for 5 min and then cast onto glass substrates and rectangular steel (Fe_3C) coupons, followed by a curing procedure at 70°C under a vacuum atmosphere for 5 h. The curing temperature was subsequently raised to 150 (for 2 h) and 250°C (for 2 h), respectively (Fig. 1).

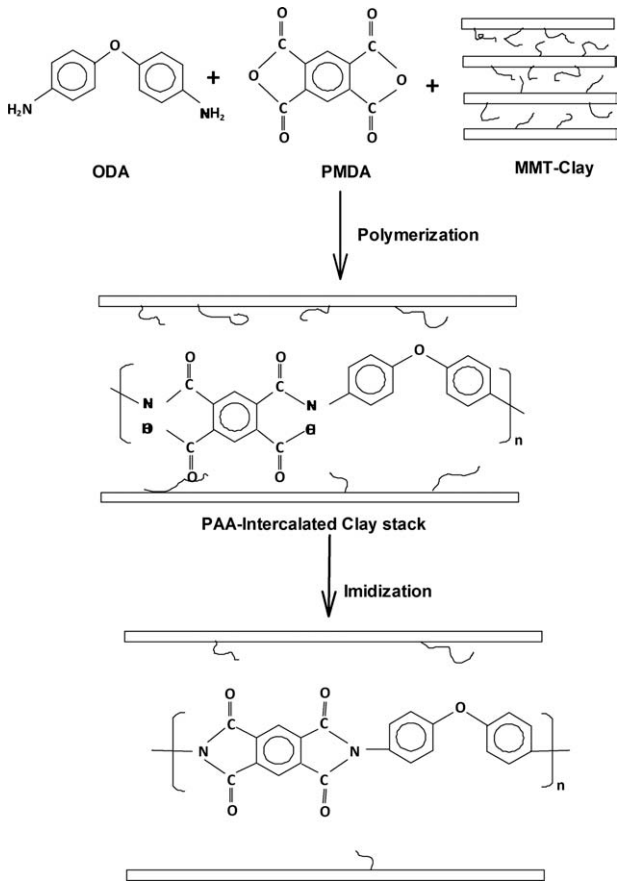

Figure 1 Preparation of PAA/nanoclay and PI/nanoclay composites.

Characterization

The progress of condensation polymerization was followed by a time-based viscosity measurement on aliquots drawn from the polymerizing solutions. The viscosity of the polymerizing solution was measured as a function of polymerization time by using the Brookfield Viscometer (DV I) at ambient temperature. The viscometer spindle speed was varied from 1 to 100 rpm. Attenuated total reflectance infrared spectroscopy (FTIR-ATR) was used to determine both the chemical structure of PAA and the extent of imidization (EOI) of PI. Spectra of the coatings and free-standing films were collected at a resolution of 4 cm^{-1} after 32 scans per sample between 4000 and 400 cm^{-1}. A background spectrum of a bare-polished steel substrate was subtracted from the acquired spectrum for the coating cast on steel.

The structure of clay was analyzed by conducting wide angle X-ray diffraction (WAXD) measurements using the Philips X-ray diffractometer at University of Cincinnati. The X-ray diffractometer is equipped with a Cu Kα radiation source. WAXD tests were

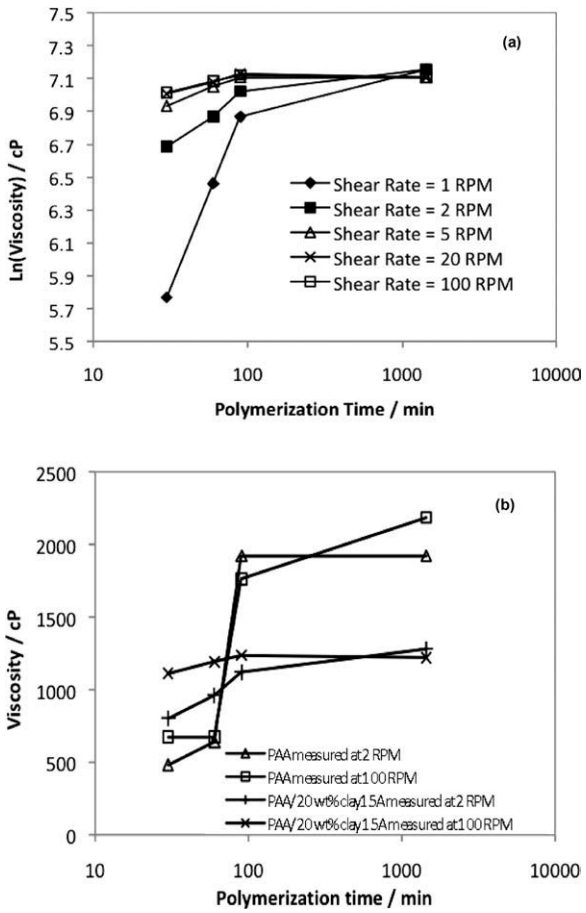

Figure 2 Change of shear viscosity as a function of polymerization time at varying spindle speeds for (a) PAA/nanoclay 15A composite; (b) comparison of PAA and PAA/nanoclay 15A during the polymerization of PAA.

carried out at a wavelength of 1.54 Å between 2θ angle of 0.5° and 10° at a scan rate of 0.005°/s.

Differential scanning calorimetry (DSC) was carried out at University of Cincinnati. About 5 mg of each sample initially cured at 70°C for 5 h was scanned from 25 up to 300°C at a heating rate of 10°C/min under nitrogen atmosphere. The thermograms were used to measure the heat of polycondensation and imidization reactions and determine the peak temperatures for the polymerization and curing.

The morphology of the free standing films was observed by using an FEI XL30 environmental scanning electron microscope (ESEM) and transmission electron microscopy (TEM). The SEM samples were coated with silver to enhance conductivity, and microscopy was performed under the environmental mode. Secondary electrons were collected at an accelerating voltage of 20 kV. The ESEM pictures of the cross-section of the films were examined at magnification up to 100 k to gain an insight into the structure and orientation of clay in the matrix. The TEM samples were prepared with copper grids and observed using A JEOL JEM 4000EX TEM at a voltage of 80 kV.

RESULTS AND DISCUSSION

Effect of nanoclay on the polymerization of PAA

Figure 2(a) shows the dependence of viscosity of the polymerizing solution on the polymerization time of ODA/PMDA at varying spindle speeds. The formation of PAA is marked by a drastic increase in the viscosity of the polymerizing solution, which approaches an asymptote at about 90 min of polymerization as shown in Figure 2(a). The initial viscosity of the polymerizing solution also increases with increasing spindle speed, indicating a non-Newtonian solution. Shown in Figure 2(b) is the comparison of time-dependent viscosity between ODA/PMDA solutions with and without the presence of clay. The polycondensation of ODA and PMDA at the absence of clay commences at a lower viscosity at short reaction times ($t \leq 30$ min) and increases sharply to a maximum value of over 1300 cP after 90 min. The ODA/clay/PMDA system starts polymerization at a significantly higher viscosity of about 1096 cP and only increased slightly after a prolonged polymerization time ($t \geq 90$ min). The steady-state viscosity of the ODA/clay/PMDA is significantly lower than that for ODA/PMDA polymerizing solution. This result indicates that the presence of clay exerts a great influence on the polymerization of PAA and leads to a significant decrease in the molecular weight of PAA. Possible reasons involve the blocking effect of clay layers dispersed in the solution that hinders intimate contacts between the monomers. Accordingly, the steady-state shear viscosity may be considered as an indicator of the clay dispersion, and lower ultimate shear viscosity affirms a more exfoliated and more uniform dispersion of clay particles.

The interaction between clay and the polymerizing PAA molecules was investigated using UV–vis. Figure 3(a) shows the UV–vis spectra for clay dispersed in NMP, PAA-NMP solution, and PAA/nanoclay composite synthesized by *in situ* condensation polymerization containing varying weight percent of clay. All three spectra show strong absorbance in the UV region between 250 and 420 nm, corresponding to the PAA molecular structure. In addition, the PAA/clay/NMP solution exhibits a characteristic broad absorption between 420 and 600 nm represented by a peak centered in the visible region around 525 nm, which is present in neither PAA nor clay solutions separately. This absorption peak is due to the π–π* transition of conjugated bonds resulted from the interaction between PAA and the organoclay. It is also associated with the presence of a radical cation formed by the interaction of a

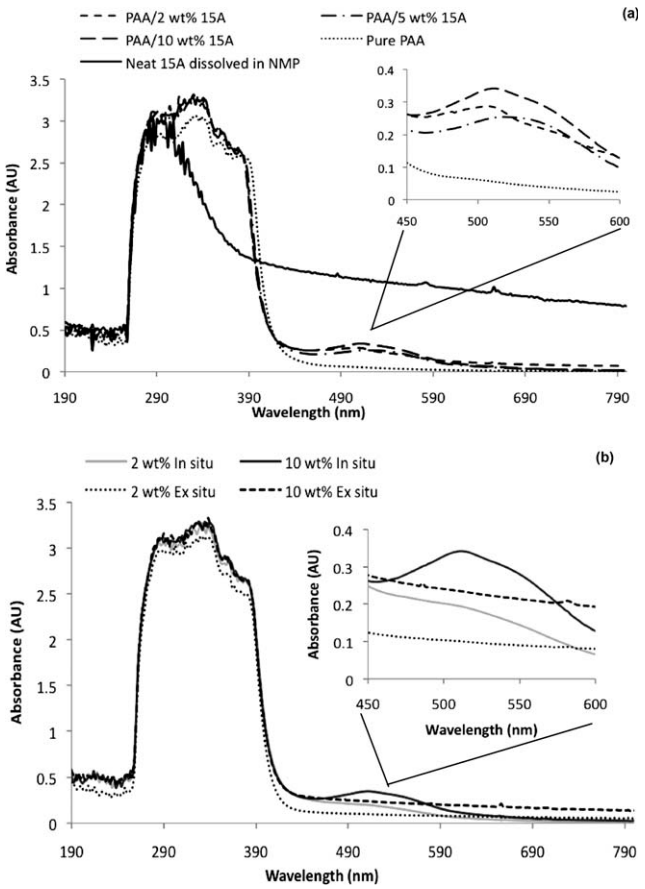

Figure 3 UV/vis spectra of (a) pure PAA, PAA/Cloisite 15A composites, and dissolved Cloisite 15A in solvent NMP; (b) UV/vis spectra of PAA/2 wt % 15A and PAA/10 wt % 15A after *in situ* and *ex situ* polymerization.

positive ion such as the alkylated quaternary ammonium ion with the carboxylic group, resulting in electron and charge delocalization.[26]

Further analysis shown in Figure 3(b) affirms this hypothesis: the PAA/clay suspension prepared by dispersing clay particles in fully polymerized PAA solutions (*ex situ*) showed no UV–vis absorption peak beyond 420 nm. However, the PAA/clay system synthesized by a one-step *in situ* condensation intercalation polymerization of PAA at the presence of clay showed the characteristic broad absorption peak around 525 nm. The intensity of this peak increased expectedly with increasing weight percent of clay. The origin of the absorption peak at 525 nm is believed to be the interaction between the PAA carbonyl group with the quaternary alkylated ammonium ion present in the clay gallery as the ion exchanger. Figure 4 shows the schematic representation of the interaction between the alkylated quaternary ammonium ion $(N^+)R_4$, which is the organic modifier in Cloisite 15A clay, and the PAA carbonyl C=O, and the creation of equivalent resonance structures of the conjugated double bonds. In this manner, PAA is doped to form a conductive charge transfer complex, and the compatibility of PAA and organoclay is greatly enhanced, which leads to highly and more uniformly dispersed clay structure.

Effect of nanoclay on the imidization behavior of PI

Imidization of PAA and PAA/nanoclay composites was performed at varying curing temperatures in order to determine how these parameters affect the EOI. A fully cured PI was obtained by heating PAA film at 300°C for 10 h under vacuum atmosphere. The characteristic IR absorption peaks and the corresponding functional groups for PI and PAA are

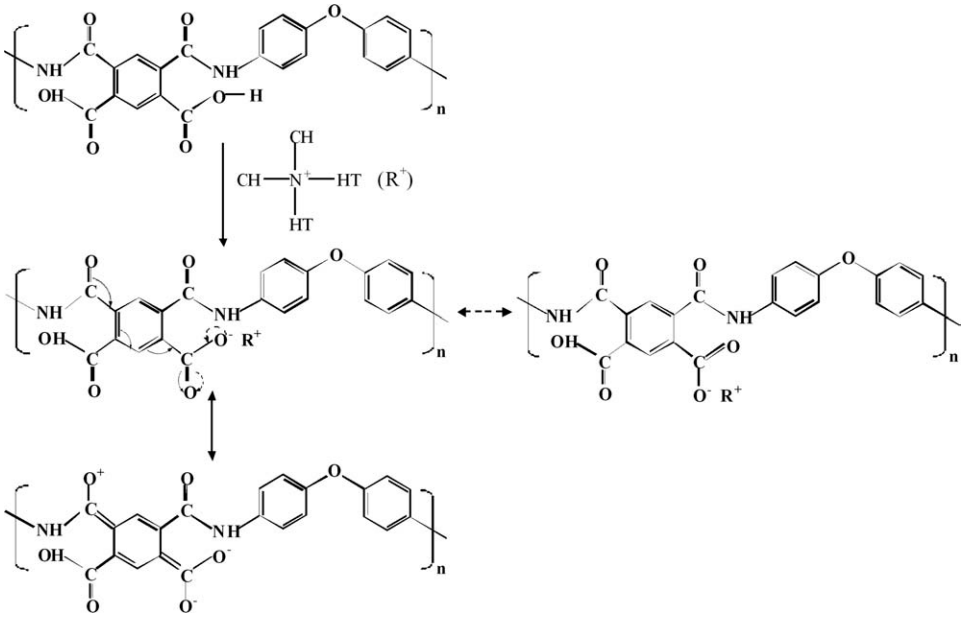

Figure 4 Formation of the conjugated structure.

TABLE I
ATR Peak Assignment for Polyimide

Frequency (cm^{-1})	Assignment
1495	Stretch (C=C—C) of aromatic ring
1778	Vibration (C=O) of imide
721	Stretch (C=O) of imide
1378	Vibration (C—N—C) of imide
588	Asymmetric stretch (C—N—C) of imide
1655	C=O of amide

tabulated in Table I.[27] IR absorption spectra for PAA/nanoclay composites cured at varying temperatures are shown in Figure 5(a). The characteristic PI absorption peaks due to the cyclic imide carbonyl were observed at 1778 and 721 cm^{-1}. Another characteristic PI absorption peak, due to the cyclic C—N—C tertiary amine functional group was observed at 1378 cm^{-1}. The cyclic imide carbonyl absorption peak at 1778 cm^{-1} was used to calculate the EOI in this study. The imide group absorption intensity was normalized using the benzene group absorption band at 1495 cm^{-1}. The EOI was calculated by using eq. (1), where "100%" refers to the fully cured PI.[28]

$$\alpha = \frac{H_{\text{imide}}/H_{\text{benzene}}}{H_{\text{imide100\%}}/H_{\text{benzene100\%}}} \quad (1)$$

As shown in Figure 5(a), the intensity of the absorption peak at 1778 cm^{-1} increased with increasing imidization temperature. The EOI of PAA/nanoclay coatings was found to be about 10% at 70°C and increased to about 25% at 110°C [Fig. 5(b)]. It, however, increased sharply to between 70 and 95% at 150°C for clay loading ranging from 2 to 20 wt %. A further increase in the curing temperature from 150 to 250°C resulted in only a moderate increase in

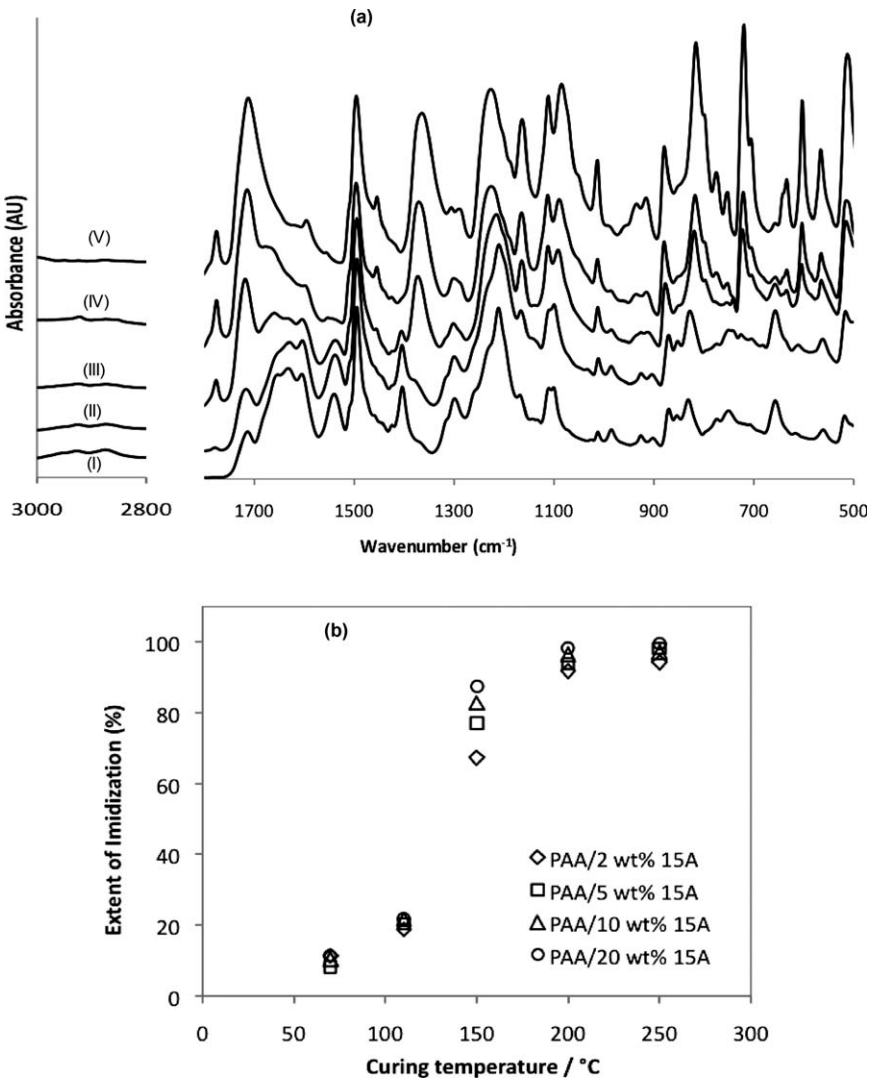

Figure 5 (a) ATR spectra of PAA/2 wt % 15A solution cast at (I) 70, (II) 110, (III) 150, (IV) 200, and (V) 250°C; (b) effect of temperature on EOI of PI.

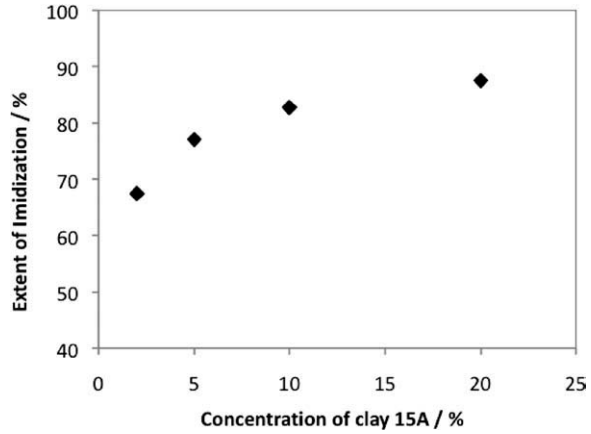

Figure 6 EOI for PAA/15A composites containing varying concentrations of 15A cured at 150°C calculated from ATR spectroscopy.

EOI to about 91–100%. As summarized in Figure 5(b), the calculated EOI showed a moderate increase at curing temperatures below 110°C and a sharp and dramatic increase between 110 and 200°C and finally a slow and marginal increase between 200 and 250°C.

EOI was calculated for PI/nanoclay composite coatings containing different clay loadings cured at 150°C as shown in Figure 6. EOI increases with increasing concentration of clay and reaches a value of about 88% for PI/nanoclay composite containing 20 wt % clay. The result indicates that the incorporation of clay into PAA by *in situ* condensation polymerization significantly improved the EOI of PI in agreement with the literature.[22] This increase in the presence of clay has been reported to result from higher surface area, which acted as available active sites for dehydration and the cyclization reactions.[29] It is also indicative that clay lowers the activation energy for imidization by facilitating the formation of hydroxonium ion, which is a better leaving group than the hydroxyl group.

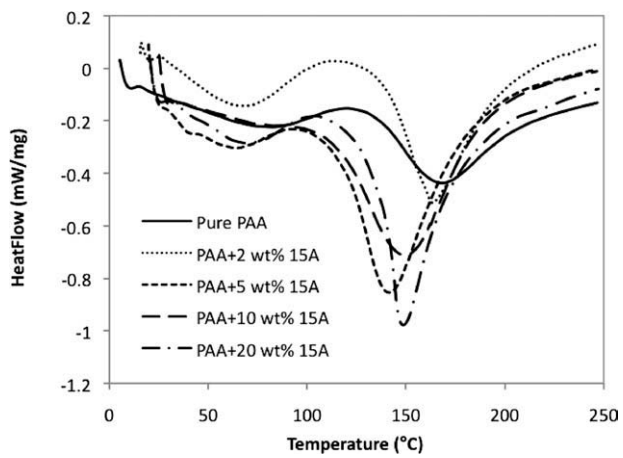

Figure 7 (a) DSC of PAA films containing 0, 2, 5, 10, and 20 wt % clay cured at 70°C.

TABLE II
Effect of Clay on the Heat and Temperature of Imidization

Clay concentration (%)	Endothermic energy (J/g)	Peak imidization temperature (°C)
0	4371.45	167.12
2	5483.53	162.64
5	6009.29	141.90
10	6635.96	148.47
20	10236.54	148.29

The thermodynamics reason for this improvement was investigated using DSC for both PAA samples with and without clay incorporation. Shown in Figure 7(a) are the first traces of the DSC thermograms for neat PI and PI/nanoclay composites containing varying weight percent of clay. A characteristic endothermic peak was observed at about 140–170°C due to cyclodehydration (imidization) reaction, with the peak temperature decreasing in the presence of clay. Also investigated was the area under the imidization endothermic peak for each sample as it was indicative of the EOI reaction. The addition of clay was observed to result in increased imidization endotherm as tabulated in Table II from 4371 to 10,236 J/g as clay content was increased from 0 to 20 wt %. It can be concluded that the presence of clay lowers (i) the imidization temperature and facilitates the imidization reaction of PAA and (ii) improves the EOI as shown by the increasing endothermic energy associated with imidization. Both phenomena are in agreement with the trend established earlier using infrared spectroscopy.

Effect of *in situ* condensation polymerization on the structure of clay

WAXD was used to detect the clay structure in clay powder, solvated clay by NMP, and PAA/clay composites cured at different temperatures. Shown in Figure 8(a), the powdered clay had three diffraction peaks at 2θ angles of 2.8°, 4.5°, and 7.2°, corresponding to the d_{001}, d_{002}, and d_{003} reflections of the clay *d*-spacing, respectively. The position of the clay diffraction peaks seems to have shifted as a result of mixed-layering of clay.[30–32] The WAXD spectrum for NMP-solvated clay, which was baked thereafter at 70°C for 2 h, showed a single broadened and weak primary peak also at 2θ of 2.8°. This result affirms that the addition of solvent has little influence on the mean *d*-spacing of clay. The drastic broadening and decrease in the intensity of this d_{001} peak suggest highly disordered clay structure associated with wide *d*-spacing distribution due to the imbibing of NMP. The solvated clay baked at 250°C

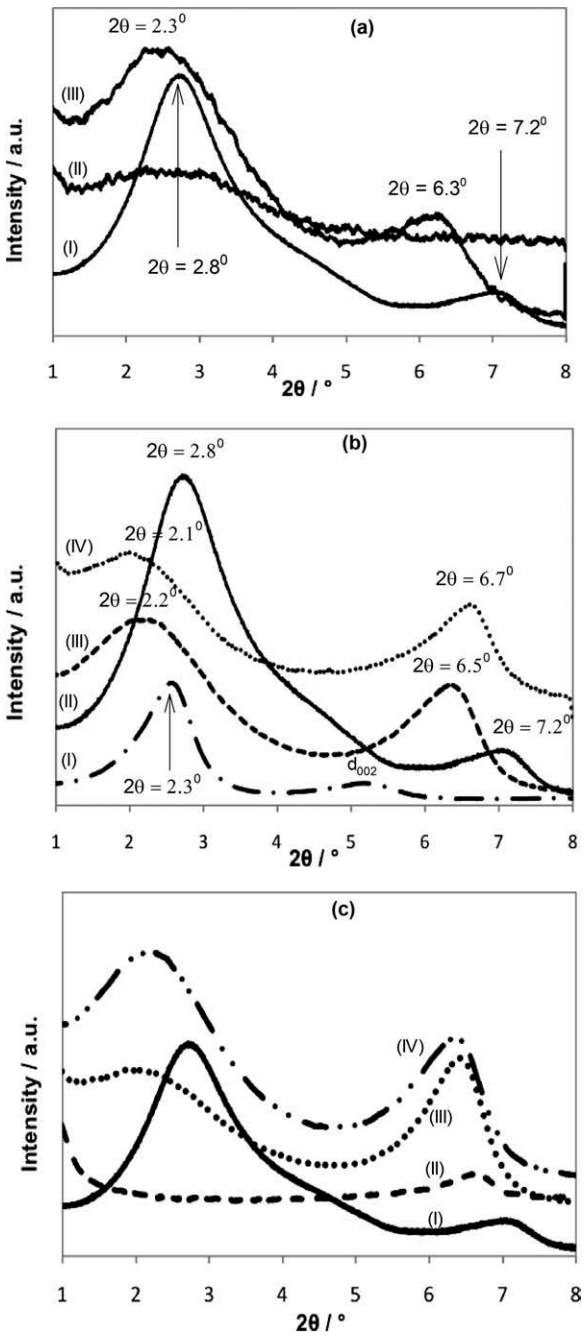

Figure 8 WAXD patterns for (a) (I) clay powder and solvated clay baked at (II) 70 and (III) 250°C; (b) (I) clay powder, and PAA/20 wt % clay composites cured at (II) 70, (III) 150, and (IV) 250°C; (c) clay powder, and 250°C-cured PAA/clay composites containing (II) 2 wt %, (III) 10 wt %, and (IV) 20 wt % clay.

showed two distinctive diffraction peaks at 2θ of 2.3° and 6.3°, respectively. The low-angle WAXD peak was broadened and shifted from 2.8° to 2.3°, corresponding to an increase in the gallery distance of 6.9 Å (31.5–38.4 Å). Highly intercalated and oriented clays were proved to present as shown by the well-resolved peak around 6.3°. This high-angle WAXD peak may reflect the narrowed clay gallery spacing as a result of partial degradation of the alkylated quaternary ammonium ion during heating up to 250°C.

The WAXD spectra for PI/nanoclay composite coatings cast on steel coupons and cured at varying temperatures are shown in Figure 8(b).

The low-angle d_{001} peak was shifted from 2.8° to 2.6°, 2.2°, and 2.1° for PI/nanoclay composite coatings cured at 70, 150, and 250°C, respectively, corresponding to d_{001} of 34.0, 40.1, and 42.2 Å, respectively. In comparison with the NMP-solvated clays, the clay *d*-spacings for the PI/nanoclay composites cured at the same temperatures are significantly larger, due to the insertion of PI into the clay gallery, which leads to better mixing and dispersion of clay in polymer matrix. Therefore, the broadening is attributed to a combination effect of (i) imbibing solvent and polymer molecules in the clay galleries and (ii) the toughening and expansion of PI molecules inside the galleries due to heating as PAA turns to PI at 250°C.

The co-existence of both low and high 2θ peaks in Figure 8(b) for PI/nanoclay composites suggests the presence of both highly intercalated (or exfoliated) clays and the clays with narrow *d*-spacing. The latter has been previously reported for polymer/nanoclay composites.[21] Literature reports claimed that the decomposition of the alkylated quaternary ammonium ion occurred at elevated curing temperatures and resulted in the narrowing of the clay gallery spacing. However, this is only true for the unintercalated clays.[21] The gallery spacing for the PI-intercalated clays during *in situ* condensation polymerization followed by imidization does not decrease, because the PI intercalate is thermally stable up to 600°C under nitrogen atmosphere.

In this study, the low 2θ d_{001} peaks located between 2° and 3° represent the PI-intercalated clays in the composites. As the curing temperature was increased to 250°C, the conversion of PAA into PI is nearly complete, resulting in stiffer and tougher PI matrix. As previously mentioned, the galleries for this group of intercalated clays broaden due to the insertion of both solvent and PAA molecules and the toughening of the intercalated polymer molecules during heating. For the high 2θ peaks, which stand for the unintercalated clays, a comparison of 250°C-cured solvated clays with and without PAA insertion [Fig. 8(a) (III) vs. Fig. 8(b) (IV)] shows the effect of PAA on the unintercalated clays apart from the decomposition of clay ions due to heating. The composite sample has a narrower *d*-spacing than the NMP-solvated clay heated at the same temperature as shown by the high 2θ angle (6.3° vs. 6.7°). Therefore, the narrowing of the unintercalated clay spacing is due to both decomposition of clay ions and the squeezing effect of the surrounded stiff PI molecules at elevated temperatures.

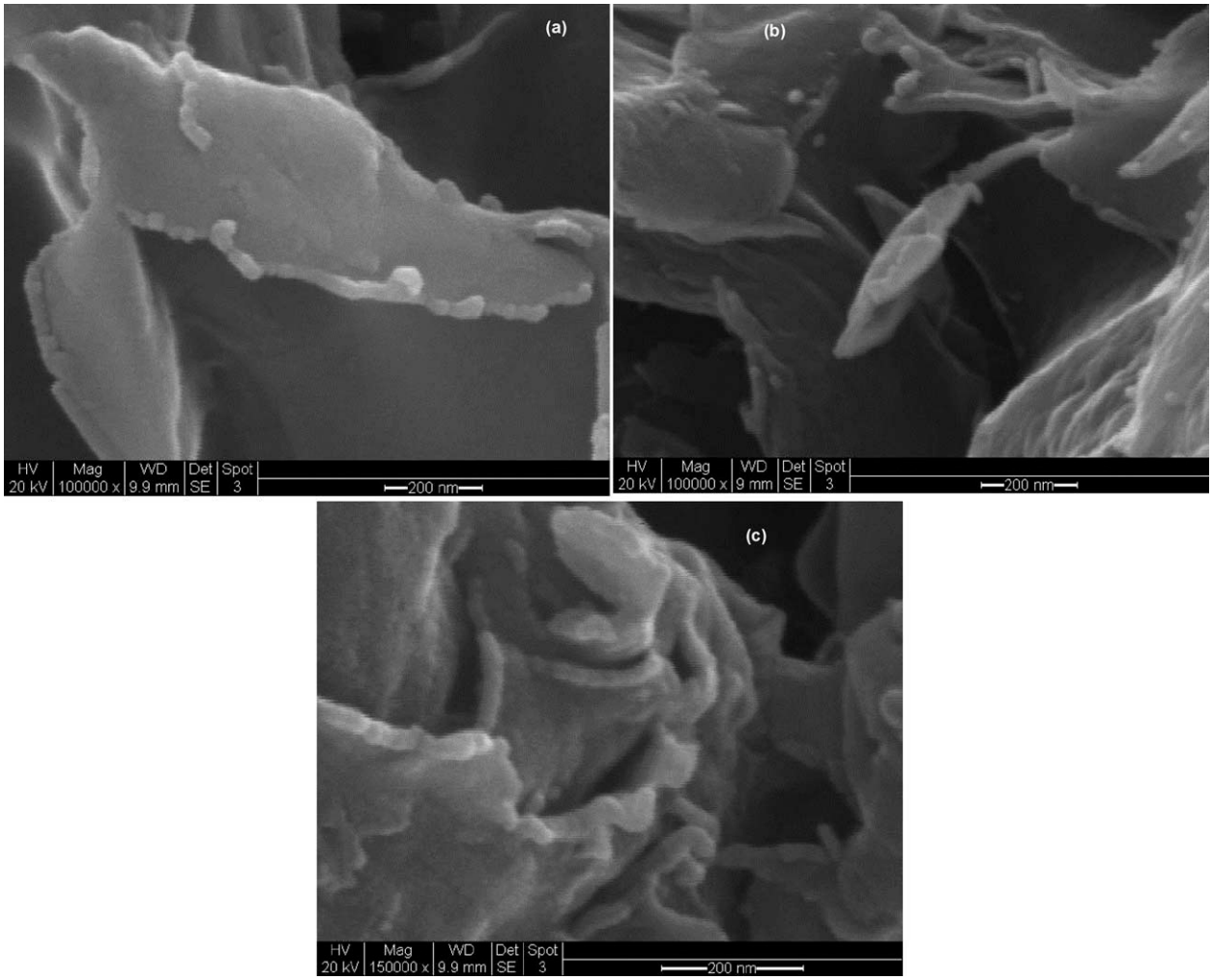

Figure 9 SEM pictures of (a) PAA/2 wt % 15A, (b) PAA/10 wt % 15A, and (c) PAA/20 wt % 15A produced by *in situ* condensation polymerization and a following curing at 250°C.

In addition, PI/nanoclay composites have higher intensity ratios of high-angle peaks ($2\theta \geq 6.1°$) to low-angle peaks ($2\theta \leq 2.8°$) than those for the NMP-solvated clays baked at the same temperatures. This phenomenon as well as the significant shift in the d_{001} peak to lower angles is due to increased extent of intercalation and orientation of clay in the presence of judiciously processed PI. *In situ* polymerization and the following curing at elevated temperatures are proved to produce highly intercalated or exfoliated and unintercalated but oriented clays.

Figure 8(c) shows that lowering the clay concentration tends to improve the intercalation of clays. This phenomenon is also affirmed by using microscopy techniques.

Morphology and structure of PI/nanoclay composites

The SEM micrographs shown in Figure 9 indicate increasing reinforcement density and alignment of clay with increasing weight percent of clay. The SEM micrographs for clay/PI composites containing lower clay concentration [Fig. 9(a,b)] show evidence of delamination of clay platelets in agreement with the WAXD results [Fig. 8(c)].

The TEM images shown in Figure 10 of the free standing films prepared from PAA/organo nanoclay composites cured at 70 and 250°C affirm the result obtained in the WAXD analysis of a co-existence of both highly intercalated (or exfoliated) and unintercalated (but oriented) clays. The image for the sample cured at 70°C is indicative of PAA-intercalated stacking clay structure with a gallery spacing of several nanometers. The clay stacks are aligned and dispersed in the matrix, while the clay stacking appear to be more compacted for the PI/nanoclay sample cured at 250°C, in which both clays with narrowed *d*-spacing and exfoliated layers can be observed.

CONCLUSION

In situ condensation polymerization of PAA in the presence of clay results in a relatively lower reaction

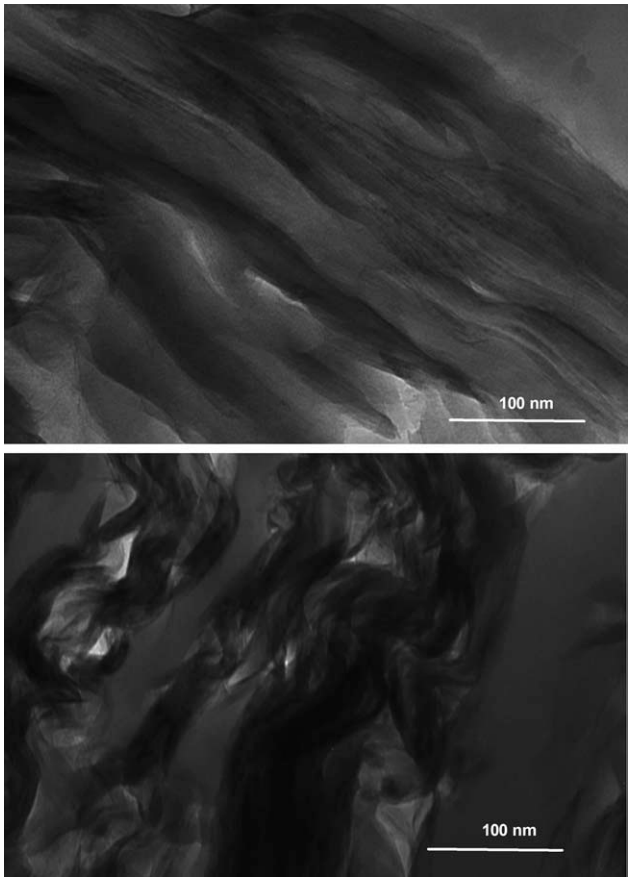

Figure 10 TEM images for PI/nanoclay composites containing 20 wt % clay cured at (a) 70 and (b) 250°C.

solution viscosity, which facilitates processing and produced PAA/nanoclay composite solutions with interesting optical activity in the visible region of the solar spectrum. The interaction between organoclay and the polymer matrix is suggested during the polymerization procedure. The dispersion of clay indicated by the *d*-spacing of clay and the viscosity of the PAA/nanoclay solution is significantly improved by *in situ* condensation polymerization method. The clay gallery spacing increased with decreasing weight percent of clay and increasing curing temperature for the PI/nanoclay coatings and thin films. Imidization of PAA is completed at lower curing temperature $T \geq 150$°C and shorter curing times in the presence of clay. The PI/nanoclay composite coatings show two sharp and intense diffraction peaks both at low diffraction angles ($2\theta < 3°$) and high angles ($2\theta \geq 6° < 7.2°$) suggesting the existence of highly intercalated and oriented clays. Exfoliation of clay is more prominent at lower weight percent of clay (lower than 10 wt %). SEM and TEM micrographs indicate that the composites contain clays that are highly intercalated and oriented.

References

1. Ahmad, Z.; Mark, J. E. Chem Mater 2001, 13, 3320.
2. Vaia, R. A.; Liu, W.; Koerner, H. J Polym Sci Part B: Polym Phys 2003, 41, 3214.
3. Pinnavaia, T. J.; Beall, G. W. Polymer-Clay Nanocomposites; Wiley: Chichester, England, 2000; 349 p.
4. Vaia, R. A.; Teukolsky, R. K.; Giannelis, E. P. Chem Mater 1994, 6, 1017.
5. Hackett, E.; Manias, E.; Giannelis, E. P. J Chem Phys 1998, 108, 7410.
6. Wang, L. Q.; Liu, J.; Exarhos, G. J.; Flanigan, K. Y.; Bordia, R. J Phys Chem B 2000, 104, 2810.
7. Usuki, A.; Kolima, Y.; Kawasumi, M.; Okada, A.; Fukushima, Y.; Kuruanchi, T.; Kamigaito, O. J Mater Res 1993, 8, 1179.
8. Giannelis, E. P. Adv Mater 1996, 8, 29.
9. Yano, K.; Usuki, A.; Okada, A.; Kurauchi, T.; Kamigaito, O. J Polym Sci A 1993, 31, 2493.
10. Ruoff, R. S.; Lorents, D. C. Carbon 1995, 33, 925.
11. Wei, C.; Srivastava, D.; Cho, K. Nano Lett 2002, 2, 647.
12. Osman, M. A.; Srivastava, D. Nanotechnology 2001, 12, 21.
13. Burnside, S. D.; Giannelis, E. P. Chem Mater 1995, 7, 1597.
14. Vaia, R. A.; Vasudevan, S.; Krawiec, W.; Scanlon, L. G.; Giannelis, E. P. Adv Mater 1995, 7, 154.
15. Fong, H.; Vaia, R. A.; Sers, J. H.; Lincoln, D.; Vreugdenhil, A. J.; Liu, W.; Bultman, J.; Chen, C. Chem Mater 2001, 13, 4123.
16. Messersmith, P. B.; Giannelis, E. P. J Polym Sci Part A: Polym Chem 1995, 33, 1047.
17. Gusev, A. A.; Lusti, H. R. Adv Mater 2001, 13, 1641.
18. Agag, T.; Koga, T.; Takeichi, T. Polymer 2001, 42, 3399.
19. Delozier, D. M.; Orwoll, R. A.; Cahoon, J. F.; Johnston, N. J.; Smith, J. G., Jr.; Connell, J. W. Polymer 2001, 43, 813.
20. Delozier, D. M.; Orwoll, R. A.; Cahoon, J. F.; Ladislaw, J. S.; Smith, J. G., Jr.; Connell, J. W. Polymer 2003, 44, 2231.
21. Nah, C.; Han, S. H.; Lee, J.; Lee, M.; Lim, S. D.; Rhee, J. M. Compos B: Eng 2004, 35, 125.
22. Tyan, H.; Liu, Y.; Wei, K. Polymer 1999, 40, 4877.
23. Lan, T.; Kaviratna, P. D.; Pinnavaia, T. J. Chem Mater 1994, 6, 573.
24. Okada, A.; Usuki, A. Mater Sci Eng, 1995, 3, 109.
25. Zeng, C.; Lee, L. J. Macromolecules 2001, 34, 4098.
26. Masters, J. G.; Sun, Y.; MacDiarmid, A. G.; Epstein, A. J Synth Met 1991, 41, 715.
27. Li, W. S.; Shen, Z. X.; Zheng, J. Z.; Tang, S. H. Appl Spectrosc 1998, 52, 985.
28. Hall, S. MS. Thesis, University of Cincinnati, 2007, p 128.
29. Ballantine, J. A.; Davies, M.; Patel, I.; Purnell, J. H.; Rayanakorn, M.; Williams, K. J.; Thomas, J. M. J Mol Catal 1984, 26, 37.
30. Causin, V.; Marega, C.; Marigo, A.; Ferrara, G. Polymer 2005, 46, 9533.
31. Eckel, D. F.; Balogh, M. P.; Fasulo, P. D.; Rodgers, W. R. J Appl Polym Sci 2004, 93, 1110.
32. Priya, L.; Jog, J. P. J Polym Sci Part B: Polym Phys 2003, 41, 31.